Available online at www.sciencedirect.com
SCIENCE DIRECT®
Journal of Catalysis 224 (2004) 441–448
JOURNAL OF CATALYSIS
www.elsevier.com/locate/jcat

Synthesis and catalytic properties of thermally and hydrothermally stable, high-surface-area SiO_2–CeO_2 mesostructured composite materials and their application for the removal of sulfur compounds from gasoline

A. Corma,[a,*] J.Y. Chane-Ching,[b] M. Airiau,[b] and C. Martínez [a]

[a] *Instituto de Technología Química, UPV-CSIC, Universidad Politécnica de Valencia, Avd de los Naranjos s/n, 46022 Valencia, Spain*
[b] *Rhodia Recherches, 52 Rue de la Haie Coq, 93 308 Aubervilliers, France*

Received 30 January 2004; revised 4 March 2004; accepted 4 March 2004

Available online 20 April 2004

Abstract

Nanostructured SiO_2–CeO_2 composite materials were prepared by embedding monodispersed, inorganic colloids in ultrafine structured layers of mineral binder using a self-assembly process. Cohesive, highly concentrated CeO_2 nanoparticle arrays, characterized by a spacing in the range of a nanoparticle diameter, were synthesized. These materials possess high surface areas and are stable to temperatures up to 800 °C by virtue of surface roughness on the nanometer scale and relatively large inorganic layer thickness. Gaseous access to the CeO_2 nanoparticle surfaces was obtained through a matching of nanoparticle sizes to the thickness of the structured layers. These SiO_2–CeO_2 nanostructured materials showed very good catalytic properties as additives for reducing sulfur concentration in gasoline through fluid catalytic cracking. We demonstrate that these thermally stable, high-surface-area arrays of CeO_2 nanoparticles are best suited for the cracking of long-chain, those which commonly present the greatest difficulty, alkylthiophenes and alkylbenzothiophenes.

Keywords: SiO_2–CeO_2 mesostructured materials; CeO_2 nanoparticles; Catalytic cracking additives; FCC gasoline sulfur reduction additives

1. Introduction

Engineering of materials at the nanometer scale has attracted much interest in the fields of electronics [1], optics [2,3], catalysis [4], and magnetism [5]. Current research interest has moved beyond the investigation of the properties of isolated nanoparticles toward the study of the properties of nanoparticle arrays [3,6,7]. Arrays of nanoparticle synthesis through self-assembly have demonstrated new collective optical, magnetic, and transport properties with properties differing from those of the isolated nanoparticle and from those of the bulk phase [6]. These self-assembled nanoparticles are generally formed through a deposition procedure based on the evaporation of solvent from a nanoparticle dispersion [8]. Alternative pathways proceed through homogeneous nucleation-crystallization processes involving the evaporation of solvents from a multisolvent dispersion, inducing nanoparticle destabilization [9]. Ordered arrays of nanoparticles with interparticle spacing within the range of 0.7 to 1.8 nm [6] are generally formed from nanoparticles with surfaces functionalized by organic groups such as alkanethiols and alkylphosphine oxides. These surface organic moieties provide a minimal internanoparticle cohesion rendering the subsequent arrays unstable to high temperatures and attrition conditions. Moreover, arrays of nanoparticles displaying high surface area are susceptible to sintering and grain growth effects at high temperatures. It is therefore a useful goal to produce high-surface-area nanoparticle arrays which are stable under high temperatures. Such arrays, displaying stable high surface areas, will have excellent potential in such areas as high-temperature catalysis.

We describe a new route for the preparation of ordered high-surface-area arrays of individualized nanoparticles which are stable in a large range of temperatures up to 800 °C. Our synthetic approach involves the self-assembly of an array of CeO_2 nanoparticles [10] embedded within ultrathin layers of highly structured SiO_2 binder. In contrast to previous studies, which typically involve nanoparticles in the range 20–30 nm [11], nanoparticles were selected with

* Corresponding author. Fax: +34 96 387 7809.
E-mail address: acorma@itq.upv.es (A. Corma).

0021-9517/$ – see front matter
doi:10.1016/j.jcat.2004.03.004

diameters of 5 nm. This size was chosen as a compromise to allow the formation of materials with high surface areas and to maximize access to the surface areas of the CeO_2 nanoparticles embedded within the thin layers of structured SiO_2 binder. Inhibition of surface area reducing, sintering, and grain growth of the nanoparticle arrays was achieved through the formation of a homogeneous distribution of nanoparticles, without internanoparticle contact, within the layers of the SiO_2 binder. The SiO_2 was selected as a mineral binder to generate high thermal stability in the nanoparticle arrays.

We will also show here that the mesostructured material is stable after calcinations at 750 °C in the presence of 1 bar steam. Such types of materials offer possibilities, among others, for catalytic processes involving high temperatures. These materials will be evaluated as additives for sulfur reduction of a vacuum gas oil under fluid catalytic cracking (FCC) conditions.

2. Experimental

2.1. Materials

The SiO_2–CeO_2 nanostructured composite material was prepared from colloidal nanoparticle CeO_2 building blocks. Ordered nanostructured composites were formed through self-assembly of monodispersed CeO_2 nanoparticles and a SiO_2 binder from an acidic homogeneous medium [10]. We adopted a process which involves the formation of mesostructured silica together with the simultaneous inclusion of CeO_2 nanoparticles. The assembly process was controlled by adjusting the interactions of a copolymer template with the CeO_2 nanoparticles and SiO_2. In order to obtain appropriate interactions with a colloid with a diameter of 5 nm, an amphiphilic poly(alkylene oxide) block copolymer $HO(CH_2CH_2O)_{20}$ $(CH_2CH(CH_3)O)_{70}$ $(CH_2CH_2O)_{20}H$ (designated $EO_{20}PO_{70}EO_{20}$) was used.

A 4.15 M CeO_2 colloidal dispersion was prepared following a procedure previously described [10]. Residual Ce^{4+} concentration of the acidic CeO_2 colloidal dispersion was reduced by ultrafiltration. After ultrafiltration, the acidity of the dispersion is determined by chemical analysis of the supernatant after ultracentrifugation at 50,000 rpm over 6 h. The molar ratio $[H^+]/[CeO_2]$, referred to as the CeO_2 nanoparticle concentration, was found to be $[H^+]/[CeO_2] = 0.025$. In a typical synthesis, 10 g of poly(alkylene oxide) block copolymer $HO(CH_2CH_2O)_{20}$ $(CH_2CH(CH_3)O)_{70}$ $(CH_2CH_2O)_{20}H$ (designated $EO_{20}PO_{70}EO_{20}$, Pluronic P 123, BASF) was dissolved in 346 cc water and 37.6 cc of HCl 2 M. The amount of 4.82 cc of the 4.15 M CeO_2 colloidal dispersion previously described was poured into this solution. Then 16.67 g of TEOS (tetraethyl orthosilicate) was added at room temperature into the dispersion with stirring for 60 mn. The resulting dispersion was aged at 45 °C for 16 h and a precipitate was formed. The mixture was then aged overnight at 80 °C without stirring. The solid product was recovered, washed by water, and air-dried at 80 °C. The copolymer template was removed by calcination, by slowly increasing the temperature from room temperature to 500 °C in 6 h and heating at 500 °C for 6 h.

2.2. V/SiO_2–CeO_2 catalyst

Calcined Si–Ce mesoporous material (500 °C) has been impregnated using an aqueous solution containing $VO(SO_4)$ to obtain a final V content of 0.75 wt% metal. The impregnation has been performed following the incipient wetness procedure. After impregnation, the material was dried at 100 °C for 6 h and calcined for 3 h at 600 °C. The calcined (Fresh) sample has been characterized and further hydrothermally treated in a muffle furnace (5 h/750 °C/100% steam) to simulate equilibrated performance in the FCC unit.

This final sample (Steamed) has been the one tested as FCC additive.

2.3. Characterization methods

Transmission electron microscopy (TEM) micrographs were obtained on a Jeol 1200X electron microscope operating at 120 keV. The samples for TEM were prepared directly dispersing the powders onto carbon copper grids.

The nitrogen adsorption and desorption isotherms at 77 K were measured using a Micromeritics ASAP 2000 system with previous overnight drying of samples under vacuum at 20 °C. For the BJH (Barret–Joyner–Halenda model), the pore-size distribution was obtained from the analysis of the desorption branch of the isotherms.

High-angle X-ray powder diffraction spectra were obtained on a Philips PW 1800 diffractometer using a Cu-K_α radiation ($\lambda = 1.54$ Å).

SAXS data were collected using the 2-m pinhole instrument of the Centre d'Etudes de Saclay, France, and were corrected for background scattering.

Concerning the propanoic acid chemisorption studies, pure SiO_2 mesoporous material was prepared according a procedure previously described [12]. Pure CeO_2 mesoporous material was prepared by self-assembly of CeO_2 nanoparticles [13]. Chemisorption of volatile propanoic acid was performed on materials poured in a chromatographic column at 110 °C through a gas flux of 20 $cm^3\,min^{-1}$. This procedure was repeated until reproducible chromatograms were obtained. A thermal treatment was then carried out at 200 °C for 2 h in order to desorb the physisorbed species.

2.4. Catalytic experiments

The SiO_2–CeO_2-based material has been tested as additive for gasoline sulfur reduction during the catalytic cracking of an Arabian light vacuum gas oil (VGO) with a sulfur content of 1.4 wt% whose properties are given in Table 1. Therefore, a 30 wt% of the additive, as referred to the amount of base catalyst, has been added and physically blended with the base. The base catalyst used is a steam-deactivated (1089 K, 11 h, 90% steam) commercial FCC

Table 1
Characteristics of the Arabian light VGO used for the MAT experiments

Density 288 K (g/cc)	0.9072					
Aniline point (wt%)	91.2					
Sulfur (wt%)	1.4					
N_2 (ppm)	890					
Average molecular weight	438					
Viscosity (c.s. at 373 K)	6.29					
Refraction index at 340 K	1.488					
CCR (wt%)	0.32					
K(UOP)	12.03					
Distillation curve *D*-1160 in wt% (K)						
IBP	5	10	30	50	70	90
(552)	(604)	(633)	(690)	(721)	(751)	(812)

catalyst which contains 1 wt% of rare earth (RE), with a BET surface area of 170 m^2/g and a zeolite unit cell size of 2.435 nm. Catalytic cracking of the VGO has been performed in an automated Microactivity test (MAT) unit, designed in accordance to the ASTM D-3907. This unit can be programmed to perform cyclic experiments (reaction, stripping, and regeneration) in a wide range of experimental conditions.

The MAT tests have been carried out at 783 K, 30 s time on stream (TOS), and catalyst to oil ratios ranging from 2 to 5 g/g referred to the amount of base catalyst (4 g). The deactivated catalyst was regenerated at 813 K for 3 h in air flow.

Gas products have been analyzed on-line with a gas chromatograph equipped with two detectors. H_2 and N_2 are detected with a thermal conductivity detector (TCD) and the hydrocarbons, up to C_6, are detected with a flame ionization detector (FID). In the reported results, the gases yield includes hydrocarbons from C_1 to C_4. The C_5 and C_6 compounds present in the gaseous products are included in the gasoline fraction. The liquids obtained have been analyzed by simulated distillation to determine the fraction of light gasoline (C_5–150.8 °C), heavy gasoline (150.8–221 °C), LCO (221–359 °C), and HCO (359+ °C). A detailed sulfur compound identification in the liquids has also been performed by gas chromatography. For this purpose the different compounds are separated by boiling point in a high-resolution capillary column (Petrocol-100), and at the outlet they are detected simultaneously with two detectors, a FID for all the compounds present in the sample, and a pulsed flame photometric detector (PFPD), a specific sulfur detector. In order to avoid the inlet of the heaviest fraction of the liquids into the analytic column, a prefractionating system is used so that compounds with boiling points higher than 286.8 °C do not enter the analytical column.

3. Results and discussion

3.1. Synthesis and characterization

Hexagonal ordering of the calcined CeO_2 arrays, embedded in ultrathin SiO_2 layers, are observed through

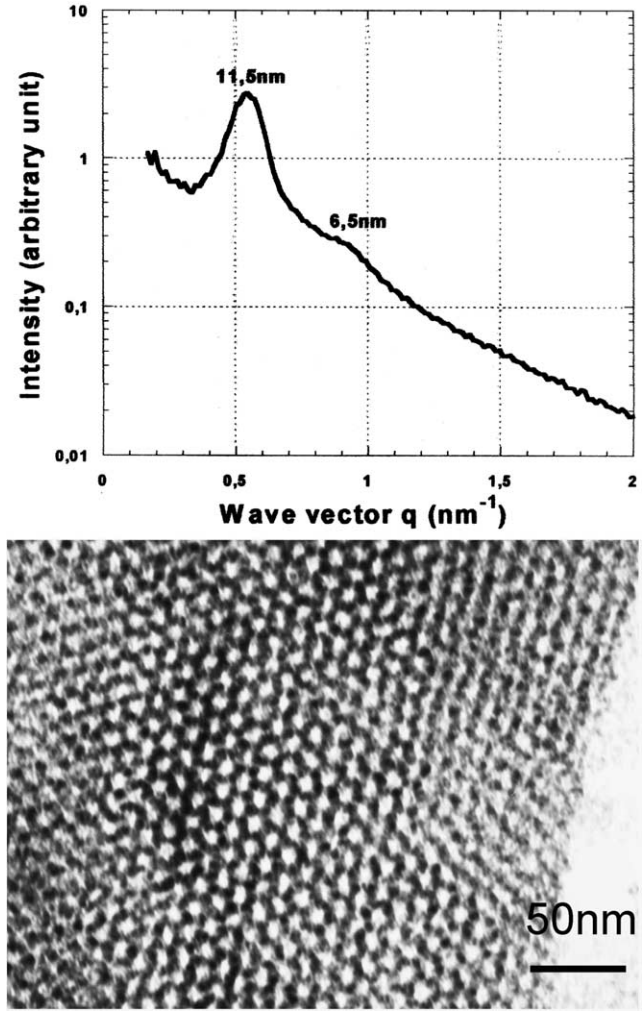

Fig. 1. Characteristics of the array made at $C_{CeO_2} = 0.2$ and calcined at 500 °C, 6 h. (Top) SAXS diffraction pattern showing an hexagonal phase. (Bottom) TEM micrograph showing a hexagonal array of pores.

SAXS when C_{CeO_2}, the molar ratio of CeO_2 ($C_{CeO_2} = [CeO_2]/[CeO_2 + SiO_2]$), is less than 0.25. The SAXS pattern, given in Fig. 1, for $C_{CeO_2} = 0.2$ shows two diffraction peaks at 11.5 and 6.5 nm which are indexed from a two-dimensional hexagonal structure with a lattice constant a of 13 nm where $a = 2d_{SAXS}/\sqrt{3}$ and d_{SAXS} is the characteristic length measured from the SAXS spectra, as the 100 and 110 peaks, respectively. Transmission electron microscopy was performed upon thin sections of the CeO_2 arrays prepared by ultramicrotomy. Well-ordered large channels with hexagonal symmetry were observed, as shown in Fig. 1. At lower magnifications the observed high-contrast inorganic walls suggest the presence of CeO_2 nanoparticles within the silica framework. At higher magnifications, the crystal planes within the CeO_2 nanoparticles could be observed (Fig. 2). Such a structure can then be described as a homogeneous distribution of CeO_2 nanoparticles in an ultrathin textured silica framework with particle to particle distances in the range of a single particle diameter. TEM micrographs of the $C_{CeO_2} = 0.2$ material reveals the existence of two

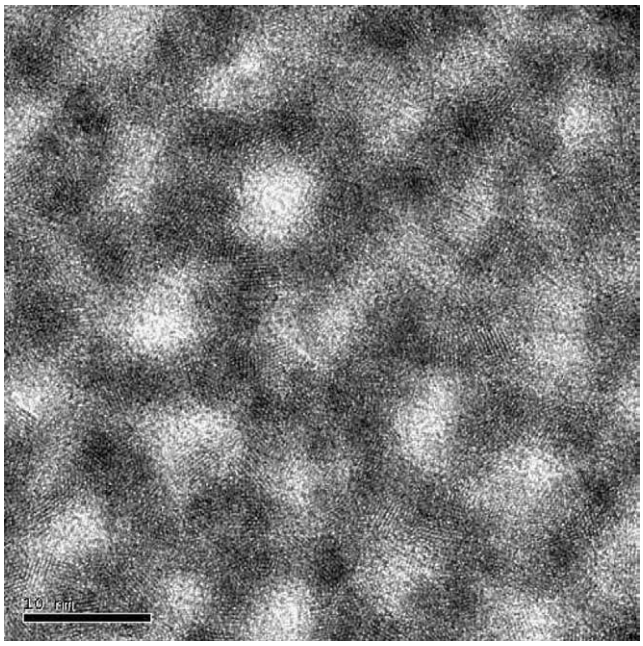

Fig. 2. TEM micrograph showing the crystal planes within the CeO_2 nanoparticles.

structured domains. The arrays of CeO_2 nanoparticles embedded within the thin silica layers give high contrast areas with large interpore distances. The other structured domain is of lower contrast with shorter interpore distances and is attributed to phase pure SiO_2. Wide-angle X-ray diffraction studies on samples calcined at 500 °C confirm the crystalline nature of the nanostructured SiO_2–CeO_2 material. High-angle X-ray Bragg peaks were observed at 28.5, 33, 47.5, and 56°, using a Cu-K_α X-ray source, characteristic values for the CeO_2 structure. The nanocrystallite size, calculated using the Scherrer equation from the 111 peak, gave a value of 4 nm, slightly lower than the nanoparticle diameter.

In contrast to previous work [11], our procedure was successfully applied to the synthesis of highly concentrated arrays of nanoparticles in an attempt to minimize the inter-nanoparticle spacings. CeO_2–SiO_2, materials were formed with greater CeO_2 concentrations with C_{CeO_2} molar ratio values up to 0.5. The successful preparation of these ordered arrays was achieved through a fine tuning of the acid molar ratio, $[H^+]/[Si + Ce]$. The desired materials form within a narrow acid molar ratio range between 0.375 and 1.5. These acid molar ratio values are greater than that for the initial colloidal dispersion of 0.025 and were achieved through the addition of HCl. The degree of order observed in the CeO_2–SiO_2 materials was probed through inspection of the SAXS spectra. CeO_2 nanoparticle arrays prepared at a C_{CeO_2} concentration of 0.50 show a single peak in their SAXS patterns, Fig. 3, indicating that they are less ordered than those formed at $C_{CeO_2} = 0.2$. The materials prepared at a C_{CeO_2} molar ratio of 0.50, prepared with similar copolymer concentration ($[OE]/[Si + Ce] = 0.68$), consist of a mixture of hexagonal and layered arrays of nanoparticles, as

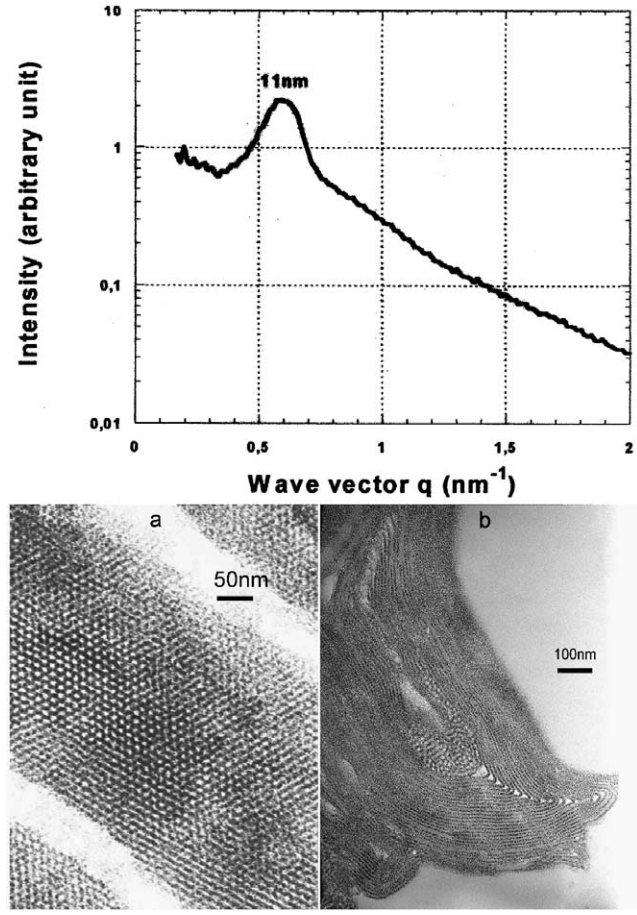

Fig. 3. Characteristics of the array made at $C_{CeO_2} = 0.5$ and calcined at 500 °C, 6 h. (Top) SAXS diffraction pattern. (Bottom) TEM micrographs showing a mixture of structures. (a) Domain displaying a hexagonal array of pores. (b) Domain exhibiting a layered structure.

shown by TEM in Fig. 3. The characteristic lengths, d_{SAXS}, observed by SAXS of 11 nm is similar to the lengths observed for the $C_{CeO_2} = 0.2$ material of 11.5 nm. Distribution of the CeO_2 nanoparticles in the thin layer of mineral was determined through high magnification TEM imaging. As observed for the $C_{CeO_2} = 0.2$ materials, the nanostructured composite material consisted of a homogeneous distribution of perfectly individualized CeO_2 nanoparticles. TEM imaging indicates a constant interparticle spacing in the range of a single nanoparticle for the material prepared at $C_{CeO_2} = 0.5$. This observation is consistent with the observed difficulty in preparing highly concentrated ordered arrays of CeO_2 nanoparticles embedded in ultrathin layers of silica and suggests the existence of a maximum C_{CeO_2} required to form this material. Our results suggest that this maximum value is approximately 0.5.

After calcination at 500 °C, BET measurements show that these highly concentrated arrays of nanoparticles have high surface areas with values up to 300 $m^2\ g^{-1}$ (1395 $m^2\ cm^{-3}$). Comparative t plots of the materials demonstrate the absence of micropores or small mesopores within the silica domains. Materials were formed with porous diameters independent

from the CeO_2 content. Pore diameters between 6.0 and 7.0 nm were measured from N_2 desorption isotherm for materials with CeO_2 molar ratios varying between $C_{CeO_2} = 0.2$ and $C_{CeO_2} = 0.5$. The characteristics lengths, determined by SAXS, and the pore diameter, derived from BET measurements, give a mineral binder thickness of 6–7 nm for all the materials. This value is slightly larger than that of the diameter of the constituent nanoparticles. The experimental surface area value, determined from the adsorption curve, was greater than estimated values derived from simple geometrical arguments which consider smooth surface walls, and a wall thickness determined from SAXS and pore-size measurements, in hexagonal and layered systems. To account for this, we investigated the topology of the surfaces by inverse chromatography. The enthalpy energies of adsorption of probe molecules with differing steric volumes (dimethylalkane or cyclic alkane molecules) onto the surface of the material were determined as a function of equivalent alkyl chain length [14,15]. A different relationship was observed between adsorption energy and equivalent alkyl chain length for linear and cyclic alkane probe molecules. The results indicate a steric exclusion effect for the cyclic alkanes probes. Since this different behavior, for the dimethylalkanes and cyclic alkanes, was not observed for a pure mesoporous SiO_2 sample, these differences were attributed to nanoscale roughness on the surfaces of the SiO_2–CeO_2 materials. This roughness could bias the pore-size determination calculated from BET experiments and contribute to the high experimentally observed surface area.

Accessibility of the CeO_2 surfaces by the gas phase, for the materials prepared at $C_{CeO_2} = 0.5$ and calcined at 500 °C, was evidenced by comparative chemisorption studies using volatile propanoic acid CH_3CH_2COOH at 110 °C with pure SiO_2 and CeO_2 mesoporous materials as references. The percentage surface coverage by propanoic acid was calculated from the surface area of SiO_2–CeO_2 materials, as measured by N_2 adsorption desorption experiments, and from the determination of the amount of grafted propanoic acid through a C elemental analysis of the chemisorbed sample. Assuming a surface coverage of 30 $Å^2$ of propanoic acid, a surface coverage ratio of 35% was determined for our SiO_2–CeO_2 nanostructured material, compared to values of 95 and 9% for the pure CeO_2 and SiO_2 materials, respectively. The values obtained for pure CeO_2 and SiO_2 materials confirm the greater affinity of the propanoic acid for CeO_2 than SiO_2 surfaces. The intermediate value determined for the SiO_2–CeO_2 materials demonstrates the surface accessibility, by a gas phase, of the CeO_2 nanoparticles embedded in the ultrafine layers.

The accessibility to the CeO_2 surfaces confirms a texturation process which involves appropriate interactions between the CeO_2 nanoparticle surfaces and the copolymer template. We propose that these interactions are stronger than those between the silica and the copolymer template. Interactions between the CeO_2 nanoparticle surface and the template were successfully achieved using an amphiphilic copolymer displaying hydrophilic moieties with a minimal number of hydrophilic EO groups with an acid-mediated route. Besides the interaction between silica surfaces and the EO moieties previously described [12], $SiOH_2^+ \ldots Cl^- H^+ \ldots OCH_2CH_2$, we proposed the following analogous interactions for the CeO_2 nanoparticles surfaces and template: $CeOH_2^+ \ldots {}^-ClH^+ \ldots OCH_2CH_2$. Selection of CeO_2 nanoparticles has the advantage of being chemically stable in the acidic medium. Under acidic conditions with large values of $[H^+]/[Si + Ce]$, undesirable ionic species such as Ce^{4+} are formed, resulting in competitive chelation of (Ce^{4+}) ions with the OE groups as described previously [16]. A minimum value of $[H^+]/[Si + Ce]$ is also required for developing an appropriate interaction with a CeO_2 colloid surface. The syntheses of these CeO_2 arrays were successfully performed for $[OE]/[Si + Ce]$ molar ratios ranging from 0.5 to 0.75. Highly structured CeO_2 arrays were obtained for $0.375 < [H^+]/[Si + Ce] < 1.5$ as previously discussed, and a $[H^+]/[OE]$ molar ratio varying from 0.5 to 1.5. This $[H^+]/[OE]$ ratio is lower than the values required for pure silica texturation [12]. These observations, together with the narrow range of experimental $[H^+]/[OE]$ values observed for the successful preparation of the nanoparticles arrays, illustrate the fine tuning required to achieve appropriate interactions with nanoparticle building blocks.

3.2. Thermal stability

The SiO_2–CeO_2 ordered materials prepared at $C_{CeO_2} = 0.5$ are stable at temperatures up to 800 °C. After calcination at 800 °C for 6 h, the desorption isotherm showed a well-defined step at $P/P_0 = 0.6$ (Fig. 4). The surface area and the pore volume of the material were determined as 175 $m^2\,g^{-1}$ (or 814 $m^2\,cm^{-3}$) and 0.24 $cm^3\,g^{-1}$, respec-

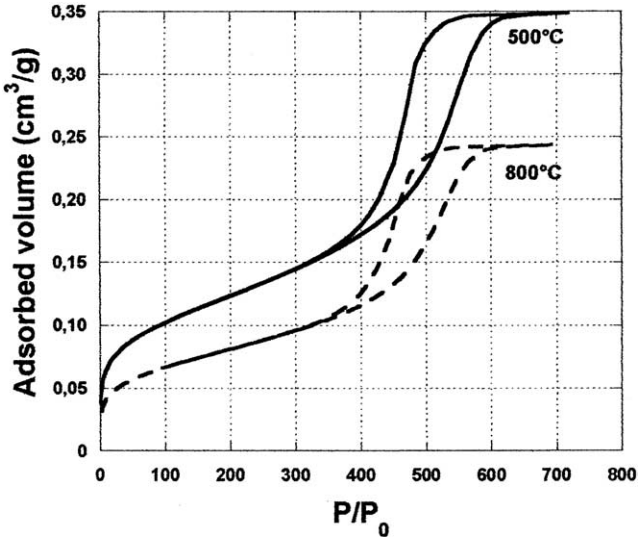

Fig. 4. Representative N_2 adsorption–desorption isotherms for the arrays assembled at $C_{CeO_2} = 0.5$ and calcined at different temperatures (500 and 800 °C).

tively. This shows that the framework is stable at this temperature, although these values are lower than those observed at 500 °C. The Debye–Scherrer formula, applied to the 111 peak, shows that the particle size of CeO_2 nanoparticles embedded in the mineral binder for the material calcined at 800 °C increases slightly to 4.5 nm, compared to 4 nm at 500 °C. This maximum temperature of 800 °C could be correlated to the maximum thermal stability of the thin silica layers [17,18], suggesting that the thermal stability of the SiO_2–CeO_2 materials is governed by the silica binder.

The hydrothermal stability of solids is a key property when they are considered for catalysis. Indeed, regeneration by coke burning involves exposure of the catalyst to steam at temperatures as high as 550 °C. However, fluid catalytic cracking catalysts are the ones requiring the highest hydrothermal stability since they are subjected in the regeneration unit to temperatures as high as 750 °C. Therefore the hydrothermal stability of a SiO_2–CeO_2 sample prepared at $C_{CeO_2} = 0.5$ and calcined at 500 °C in a first step was studied. It was treated at 750 °C with 100% steam for 5 h at atmospheric pressure and the results presented in Table 2 show that steaming produces a decrease of the surface area to 145 m^2/g. After impregnation of the fresh SiO_2–CeO_2 material with a $VO(SO_4)$ aqueous solution, the resultant material was subjected to a thermal treatment at 600 °C, and also hydrothermally treated in the same conditions as previously reported. In this case the surface area and pore volume were determined as 130 m^2/g and 0.170 cm^3/g, respectively, demonstrating the hydrothermal stability of these nanostructured composites (see Table 2). Still, both samples retain a surface area of $\sim 140\ m^2\,g^{-1}$, which renders them into quite hydrothermally stable materials.

3.3. Catalytic results: sulfur removal during fluid catalytic cracking

Sulfur in gasoline and diesel is expected to be reduced in the coming years down to 10 and 50 ppm, respectively [19]. This initiative will directly improve the air quality by reducing SO_x emissions, but will also indirectly reduce the NO_x and hydrocarbon emissions by allowing automotive catalytic converters to work better.

In the case of gasoline, the stream coming from the fluid catalytic cracking unit is the major contributor to the sulfur content in the gasoline pool [20]. Indeed, with sulfur levels as high as 1000 ppm and taking into account that FCC gasoline represents 30–40% of the total gasoline produced, it is of interest to reduce the sulfur in gasoline using FCC additives.

Two types of FCC sulfur removal additives are the most interesting commercially. One of them is based on ZnO on Al_2O_3 or in hydrotalcites [21–25], and the second one uses vanadium exchanged in Y zeolite [26,27]. The largest sulfur removal with present additives is in the 25% level, and we thought that due to the high hydrothermal stability of SiO_2–CeO_2 and its tolerance to vanadium, this could be an excellent sulfur-removal additive that, besides removing sulfur, could introduce some conversion due to its regular mesoporous structure and mild acidity [28,29], as well as SO_2 to SO_3 catalytic oxidation properties for sulfur removal with SO_x-trapping additives.

For checking the catalytic cracking properties of V/SiO_2–CeO_2 as additive, the blend formed by adding 30 wt% of this material to the base catalyst was compared with 100% of the base catalyst. The results presented in Fig. 5 show that MAT activity (gasoline + gases + coke) increases by almost 10 points conversion when introducing the additive, with the selectivity to gases and coke slightly lower and higher, respectively, when compared with the base catalyst (Table 3).

It is very interesting from the point of view of the increasing demand in $C_3 + C_4$ olefins that ratios of propylene to propane, total butenes to butanes, and more specifically isobutane to isobutane are higher when the V/SiO_2–CeO_2 additive is introduced (see Table 3). This certainly is a very interesting behavior, indicating that the additive is not only catalytically active, but it produces a larger proportion of the most desirable C_3 and C_4 olefins.

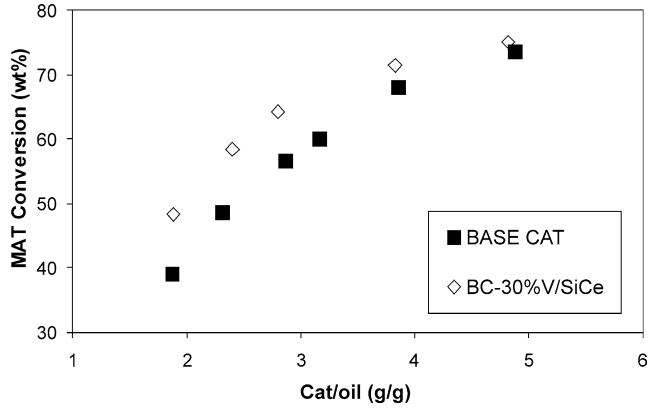

Fig. 5. MAT conversion obtained for base catalyst alone (black symbols) and blended with 30 wt% V/Si–Ce additive (0.75 wt% V) (open symbols) in catalytic cracking of a VGO in a MAT unit. $T = 510$ °C, TOS = 30 s, Cat/oil = 2–6 g/g.

Table 2
Hydrothermal stability of Si–Ce materials; surface area and pore volume of the calcined and steamed samples

Sample	BET surface area (m^2/g)	Total pore volume (cm^3/g)
SiO_2–CeO_2 (Si–Ce) calcined	310	0.261
0.75 wt% V/Si–Ce calcined	225	0.230
SiO_2–CeO_2 (Si–Ce) steamed	145	0.164
0.75 wt% V/Si–Ce steamed	130	0.170

Table 3
Selectivities obtained for base catalyst alone and blended with 30 wt% V/Si–Ce additive (0.75 wt% V) in catalytic cracking of a VGO in a MAT unit (MAT conversion = 70 wt%, $T = 510\,^{\circ}C$, TOS = 30 s)

Catalyst	Base catalyst (BC)	BC + 30 wt% V/Si–Ce
Cat/oil[a]	4.2	3.6
Gases yield (wt%)	20.2	18.9
Gasoline yield (wt%)	43.8	41.9
Coke yield (wt%)	6.0	9.2
$C_3^=/C_3$ ratio	3.4	3.8
$C_4^=/TC_4$ ratio	0.7	0.8
i-$C_4^=$/i-C_4 ratio	0.16	0.20

[a] Cat/oil is defined as ratio of total amount of base catalyst divided by total amount of gas oil fed.

Table 4
Gasoline sulfur level and product distribution in gasoline and in the C5-286.8 °C liquid fraction obtained for base catalyst alone and blended with 30 wt% V/Si–Ce additive (0.75 wt% V) in catalytic cracking of a VGO in a MAT unit (MAT conversion = 70 wt%, $T = 510\,^{\circ}C$, TOS = 30 s)

Sulfur product distribution in gasoline (ppm)	Base catalyst (BC)	BC + 30 wt% V/Si–Ce
Mercaptanes	83	102
Thiophene	74	48
Tetrahydrothiophene	55	23
C_1-thiophenes	236	164
C_2-thiophenes	114	77
C_3-thiophenes	63	26
C_4-thiophenes	168	27
Benzothiophene	820	663
Sulfur product distribution in C5–286.8 °C fraction (ppm)	**Base catalyst (BC)**	**BC + 30 wt% V/Si–Ce**
Tb > 221 °C	543	327
Benzothiophene	562	452
C_1-benzothiophene	2727	2183
C_2-benzothiophene	4516	3593
C_3-benzothiophene	4862	3875
wt% of initial S ended up as coke sulfur	0.6	7.2

With respect to sulfur removal from gasoline (see Table 4), the introduction of the additive reduces by ∼ 35% the sulfur content, and the sulfur mass balance shows that it is reduced from thiophene, tetrahydrothiophene, and alkylbenzothiophenes. Moreover, this extra sulfur eliminated from the fuels ends up into the coke (Table 4). Vanadium species may act as a Lewis acid that adsorbs higher molecular weight sulfur-containing compounds that end up as coke, instead of reacting to give alkylthiophenes and benzothiophene that will be accumulated in the gasoline. Sulfur in coke is avoided to go into the air during coke burn-off in the regenerator, by means of the widely used FCC SO_x additives. In SO_x additives, it is advised to introduce CeO_2 to catalyze the oxidation of SO_2 to SO_3 in the regenerator [30]. Thus, the SO_3 is trapped in the form of sulfate by means of a basic additive, as, for instance, hydrotalcites [31]. We have observed that the structured CeO_2 nanoparticles are an excellent catalyst for performing the oxidation of SO_2 to SO_3, adding this value to the previously presented beneficial effect on conversion, $C_3 + C_4$ olefin yield increase, and sulfur removal from the gasoline.

4. Conclusions

We have presented a mesostructured material formed by self-assembling nanoparticles. This material shows a remarkable surface area and stability which opens new possibilities for application as support/catalyst.

We have presented here one extreme catalytic application in which very high hydrothermal stability is required.

Thus, when supporting vanadium and used as an FCC additive it converts feed, while increasing the yield to C_3 and C_4 olefins. Moreover, it decreases sulfur in gasoline by ∼ 35%, and catalyses the oxidation of SO_2 into SO_3 in the regenerator as the necessary step to produce SO_x trapping by a base additive.

Acknowledgments

We are thankful to Olivier Spalla and Olivier Taché (Centre d'Etudes de Saclay, France) for their help in SAXS measurements, to Alain Thorel (Centre del Matériaux Pierre-Marie Fourt, Ecole del Mines Evry, France) for the high-magnification TEM micrograph, to Elisabeth Schweitzer and J.M. Donetti for nitrogen adsorption experiments, to Annie Vacher and Yvan Montardi for TEM observations, to E. Brendlé and F. Ozil (IGLab, Pulversheim, France) for inverse chromatography measurements, and to Howard Harvey for helpful discussions.

References

[1] M.A. Kastner, Phys. Today 46 (1993) 1.
[2] L.E. Brus, Appl. Phys. A 53 (1991) 465.
[3] A.P. Alivisatos, Science 271 (1996) 933.
[4] L.N. Lewis, Chem. Rev. 93 (1993) 2693.
[5] T. Sato, T. Iijima, M. Seki, N. Inagaki, J. Magn. Magn. Mater. 65 (1987) 252.
[6] M.P. Pileni, J. Phys. Chem. B 105 (2001) 3358.
[7] L. Motte, F. Billoudet, M.P. Pileni, J. Phys. Chem. 99 (1995) 16425.
[8] S.A. Harfenist, Z.L. Wang, M.M. Alvarez, I. Vezmar, R.L. Whetten, J. Phys. Chem. 100 (1996) 13904.
[9] C.B. Murray, C.R. Kagan, M.G. Bawendi, Science 270 (1995) 1335.
[10] J.Y. Chane-Ching, EP 208 580 (1987).
[11] D. Khushalani, S. Hasenzahi, S. Mann, J. Nanosci. Nanotechnol. 1 (2001) 129.
[12] D. Zhao, Q. Huo, J. Feng, B. Chmelka, G. Stucky, J. Am. Chem. Soc. 120 (1998) 6024.
[13] J.Y. Chane-Ching, F. Cobo, WO 0149606 (1999).
[14] E. Brendlé, E. Papirer, J. Colloid Interface Sci. 194 (1997) 207.
[15] E. Brendlé, E. Papirer, J. Colloid Interface Sci. 194 (1997) 217.
[16] W. Zhang, B. Glomski, T. Pauly, T. Pinnavaia, Chem. Commun. (1999) 1803.
[17] L.Y. Chen, S. Jaenicke, G.K. Chuah, Micropor. Mater. 12 (1997) 323.
[18] J.M. Kim, J.H. Kwak, S. Jun, R. Ryoo, J. Phys. Chem. 99 (1995) 16742.
[19] C. Marcilly, J. Catal. 216 (2003) 47.

[20] S.W. Shorey, D.A. Lomas, W.H. Keesdom, Hydrocarbon Process. 78 (1999) 43.
[21] R.F. Wormsbecher, G. Kim, US patent 5 376 608 (1994).
[22] M.S. Ziebarth, M.A. Amiridis, R.H. Harding, R.F. Wormsbecher, EP 0 798 362 (1997).
[23] T. Myrstad, B. Boe, H. Engan, E. Rytter, A. Corma, F. Rey, WO 9949001 (1999).
[24] M. Perez-Pascual, T. Myrstad, M. Hoffmeister, A. Corma, M. Boutonnet, Erdöl Erdgas Kohle 114 (1998) 605.
[25] T. Myrstad, H. Engan, B. Seljestokken, E. Rytter, Appl. Catal. A 187 (1999) 207.
[26] A.W. Chester, H.K.C. Timken, T.G. Roberie, M.S. Ziebarth, GB 2341101-A (2000).
[27] W.C. Cheng, T.G. Roberie, H.K.C. Timken, S.K. Purnell, X. Zhao, A.W. Chester, M.S. Ziebarth, GB 2345293-A (2000).
[28] A. Corma, M.S. Grande, V. González-Alfaro, A.V. Orchilles, J. Catal. 159 (1996) 375.
[29] A. Corma, V. Fornés, J. Martínez-Triguero, S.B. Pergher, J. Catal. 186 (1999) 57.
[30] K. Gwan, EP 0554968 (1993).
[31] A. Corma, A.E. Palomares, F. Rey, F. Márquez, J. Catal. 170 (1997) 140.